JACS
JOURNAL OF THE AMERICAN CHEMICAL SOCIETY

Article

pubs.acs.org/JACS

Open Access on 08/21/2015

Amino Acid Sequence in Constitutionally Isomeric Tetrapeptide Amphiphiles Dictates Architecture of One-Dimensional Nanostructures

Honggang Cui,[†,#] Andrew G. Cheetham,[∥] E. Thomas Pashuck,[†] and Samuel I. Stupp*[,†,‡,∥,§,⊥]

[†]Department of Materials Science and Engineering, [‡]Department of Chemistry, [§]Department of Medicine, and [⊥]Department of Biomedical Engineering, Northwestern University, 2220 Campus Drive, Evanston, Illinois 60208, United States

[∥]Simpson Querrey Institute, Northwestern University, Chicago, Illinois 60611, United States

Supporting Information

ABSTRACT: The switching of two adjacent amino acids can lead to differences in how proteins fold thus affecting their function. This effect has not been extensively explored in synthetic peptides in the context of supramolecular self-assembly. Toward this end, we report here the use of isomeric peptide amphiphiles as molecular building blocks to create one-dimensional (1D) nanostructures. We show that four peptide amphiphile isomers, with identical composition but a different sequence of their four amino acids, can form drastically different types of 1D nanostructures under the same conditions. We found that molecules with a peptide sequence of alternating hydrophobic and hydrophilic amino acids such as VEVE and EVEV self-assemble into flat nanostructures that can be either helical or twisted. On the other hand, nonalternating isomers such as VVEE and EEVV result in the formation of cylindrical nanofibers. Furthermore, we also found that when the glutamic acid is adjacent to the alkyl tail the supramolecular assemblies appear to be internally flexible compared to those with valine as the first amino acid. These results clearly demonstrate the significance of peptide side chain interactions in determining the architectures of supramolecular assemblies.

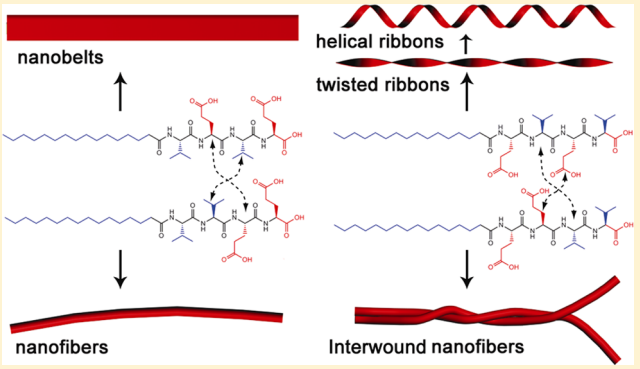

INTRODUCTION

Constitutional isomers are molecules identical in chemical composition but differing in the connectivity of their chemical bonds, often presenting very different physical properties. In one example, *n*-butanol, a chemical compound commonly used as an ingredient in perfumes or as a solvent in food and manufacturing industries, is a colorless liquid with a melting point of −90 °C, while *tert*-butanol tends to be a solid at ambient temperature with a melting point slightly above 25 °C. This difference in physical properties can be traced to the connectivity difference of chemical bonds within different constitutional isomers. In polymer science, the connectivity sequence between monomers—its tacticity—has long been known to have a significant impact on the resulting properties. For example, isotactic and syndiotactic polypropylene can crystallize into different forms due to the orientation difference of their respective side chains relative to the backbone, and the high crystallinity allows polypropylene to be used as an engineering plastics. In sharp contrast, atactic polypropylene has very low crystallinity and can only be used as an amorphous rubbery material. In biology, the switching of two adjacent amino acids often leads the protein to fold differently, causing biological malfunction or complete loss of function. Inspired by the structure−property/function correlation among various constitutional isomers, we report here the use of isomeric tetrapeptides to explore their ability to instruct supramolecular architecture in the nanostructures they form.

One-dimensional biomolecular nanostructures of soft matter are of great interest in regenerative medicine since their ability to entangle into 3D networks allows for the creation of hydrogels that can structurally and functionally mimic extracellular matrices.[1−7] Over the past decade, oligopeptides have been recognized as a very useful molecular building unit for constructing self-assembling 1D nanostructures. Interesting examples include peptide fibrils,[8−16] cylindrical nanofibers,[17−23] helical fibers,[24] twisted ribbons,[25−27] helical ribbons,[28,29] nanobelts,[25,30−32] and nanotubes.[33−38] Access to this broad range of 1D morphologies is a direct consequence of the design versatility of the peptide primary structure. However, a precise understanding of how the peptide primary structure leads to a specific supramolecular architecture is still a subject in its early stages.

Received: July 11, 2014
Published: August 21, 2014

   dx.doi.org/10.1021/ja507051w | J. Am. Chem. Soc. 2014, 136, 12461−12468

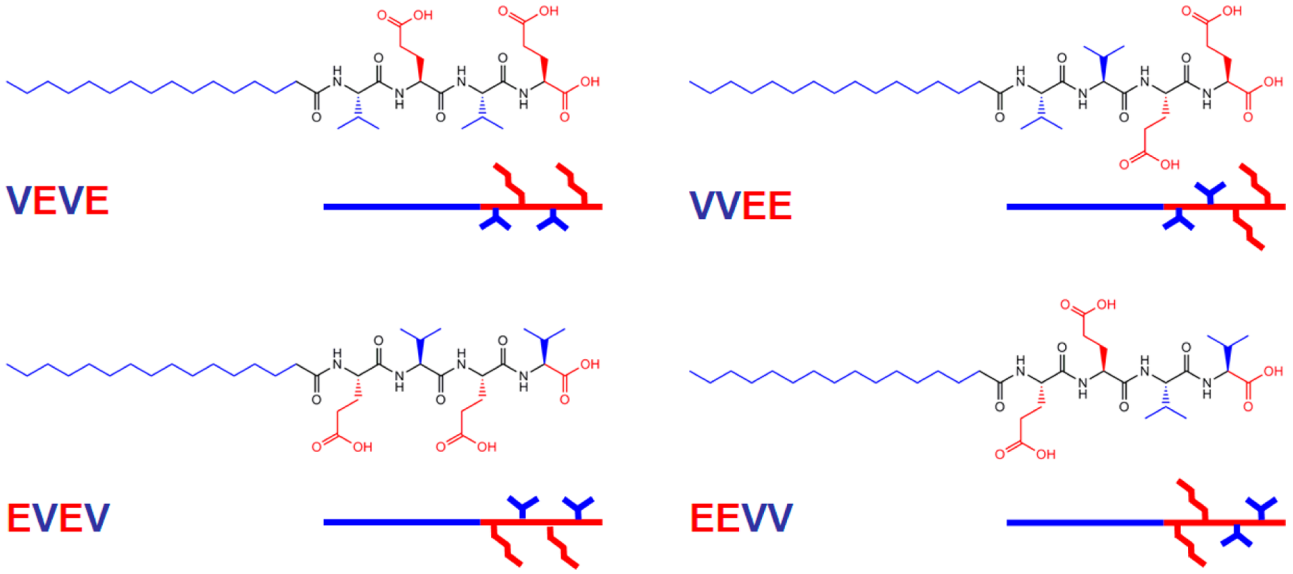

Figure 1. Molecular structures and schematic representation of the isomeric peptide amphiphiles utilized for this study. The chain conformations of the peptide segments are drawn based on the observation of β-sheet secondary structure from CD measurements (Figure S2).

Our laboratory has synthesized over the past several years a series of peptide amphiphiles (PAs) by incorporating a short hydrophobic block, in most cases an alkyl chain, onto one end of a short peptide sequence that is overall hydrophilic.[39,20,40−42] The major segment of this short peptide sequence—the part that is immediately adjacent to the hydrophobic alkyl—is generally composed of hydrophobic amino acids that have a strong propensity to form intermolecular hydrogen bonding.[2,6] In aqueous solution, these molecules tend to self-assemble into cylindrical nanofibers as a result of the combined effect of intermolecular hydrogen bonding among the peptide segments and the hydrophobic collapse of alkyl tails.[2,42] Our previous studies have shown that when a sufficient number of β-sheet-forming hydrophobic amino acids are included in the molecular design the cylindrical shape of the nanofibers is remarkably tolerant to the choice of the peptide sequence.[43] Recently, we found that this peptide region can be modified to manipulate the shape of their self-assembled nanostructures and reported a nanobelt morphology formed by self-assembly of peptide amphiphiles with a specific sequence consisting of alternating hydrophobic and hydrophilic amino acids.[25,30] We also found that other 1D morphologies such as twisted ribbons and helical ribbons can be formed by self-assembly of a PA containing a triphenylalanine segment.[44] Work from other research laboratories also suggests that self-assembling nanostructures other than cylindrical nanofibers could be accessed by variation of the peptide contour lengths,[45] or by use of a peptide containing a proline residue[46,47] or a phenylalanine residue[48] in the PA design. These results reveal the possibility of controlling the morphology of 1D nanostructure through rational choices of amino acid sequence. In this paper, we demonstrate for the first time that, by only switching the amino acid order within a tetrapeptide amphiphile, a variety of 1D morphologies can be produced, including nanobelts, single and bundled nanofibers, twisted ribbons, helical ribbons, and nanotubes.

EXPERIMENTAL SECTION

Synthesis and Purification of Peptide Molecules. All the peptides used in this study were synthesized using standard 9-fluorenylmethoxycarbonyl (Fmoc) solid phase peptide synthesis on the 1 mmol scale using Wang resin (EMD Biosciences). Fmoc deprotections were performed with 30% piperidine−DMF solution for 10 min. Amino acid coupling reactions were carried out using a coupling mixture of amino acid/HBTU/DIEA (4:3.95:6 relative to the resin) in DMF. Cleavage of the peptides from the Wang resin was carried out with a mixture of trifluoroacetic acid (TFA)/triisopropylsilane (TIS)/H_2O in a ratio of 95:2.5:2.5 for 3 h. Excess TFA and scavengers were removed by rotary evaporation. The remaining peptide solution was triturated with cold diethyl ether, the precipitate was centrifuged, and the supernatant liquid was removed by decantation. After washing with diethyl ether (three times) to remove residual TFA, the precipitate was dried under vacuum overnight. The peptides were purified by preparative RP-HPLC using a Phenomenex Gemini column (C18, 10 μm, 100 Å, 30 mm × 150 mm) at 25 °C on a Varian Prostar Model 210 preparative HPLC system. A water/acetonitrile gradient containing 0.1% v/v NH_4OH was used as an eluent at a flow rate of 25 mL/min. The purified fractions were collected and concentrated by rotary evaporation to remove acetonitrile, then lyophilized, and stored at −20 °C. The peptides were later characterized by electrospray ionization mass spectrometry (ESI-MS) using an Agilent 6520 quadrupole time-of-flight (Q-Tof) instrument, with 0.1% v/v NH_4OH in a water−acetonitrile mix (70:30) as eluent.

Cryogenic Transmission Electron Microscopy. Cryo-TEM imaging was performed on a JEOL 1230 microscope, operating at 100 kV. For cryo-TEM sample preparation, a small droplet of the solution (5−10 μL) was placed on a holey carbon film supported on a TEM copper grid. The grid was held by a tweezer mounted on a Vitrobot VI equipped with a controlled humidity and temperature environment. The specimen was blotted using preset parameters and plunged into a liquid ethane reservoir cooled by liquid nitrogen. The vitrified samples were carefully transferred to a Gatan 626 cryo-holder through a cryo-transfer stage cooled by liquid nitrogen. During observation of the vitrified samples, the cryo-holder temperature was maintained typically below −170 °C. The images were recorded with a CCD camera.

Staining-and-Drying Transmission Electron Microscopy. TEM samples were prepared as follows: a small volume (~5 μL) of dilute solution was deposited onto a carbon-coated copper grid. The excess of the solution was quickly wicked away by a piece of filter paper, and the sample was subsequently left to dry. Once dried, the samples were negatively stained by placing a drop of 2 wt % uranyl acetate aqueous solution on the top, and the excess was quickly blotted away to leave a thin layer of uranyl acetate solution. Again, the samples

dx.doi.org/10.1021/ja507051w | J. Am. Chem. Soc. 2014, 136, 12461−12468

were left to dry under ambient conditions. Bright-field TEM imaging of the assembled structures was performed on a JEOL 1230 Transmission Electron Microscope, operating at 100 kV.

Small Angle X-ray Scattering. SAXS experiments were performed using beamline 5ID-D, of the Dupont-Northwestern-Dow Collaborative Access Team (DND-CAT) Synchrotron Research Center at the Advanced Photon Source (APS), Argonne National Laboratory (ANL). The X-ray energy (15 keV) was selected using a double-crystal monochromator. The SAXS CCD camera was offset in order to achieve a wide range of scattering angle. Liquid samples were placed in 2.0 mm quartz capillary tubes. Samples were irradiated for 4 s, and the scattered radiation was detected using a marCCD detector. The 1D scattering profiles were obtained by radial integration of the 2D patterns, with scattering from the capillaries subtracted as background. Scattering profiles were then plotted on a relative scale as a function of the scattering vector $q = (4\pi/\lambda)\sin(\theta/2)$, where θ is the scattering angle.

Wide-Angle X-ray Diffraction. 2D diffraction patterns were measured at BioCARS (APS beamline in ANL, 14-BM-C) with an ADSC Quantum-315 detector. The X-ray energy of 12.668 keV (0.979 Å) was selected using a bent Ge(111) monochromator, and the beam was focused using a bent conical Si-mirror. Each scattering profile was collected for 60 s from 2.5 wt % peptide aqueous solutions that were loaded in quartz capillaries (2.0 mm in diameter). The sample-to-detector distance was 600 mm. To achieve oriented fiber diffraction, a syringe−needle system was used to carefully apply a shear force when loading the liquid samples into capillaries.

RESULTS AND DISCUSSION

To explore the effect of sequence isomerism on the self-assembly of small peptide amphiphiles, we designed and synthesized the four peptide amphiphiles shown in Figure 1. Each possesses a palmitoyl tail covalently bonded to a tetrapeptide consisting of two glutamic acid (E) and two valine (V) residues. In this particular molecular design, we chose valine due to its high propensity to form the β-sheet secondary structure and glutamic acid for its hydrophilicity and charged nature at neutral pH. Circular dichroism (CD) measurements confirm that all four PAs assume a β-sheet secondary structure in aqueous solution (Figure S2). It is expected, therefore, that the side chains of adjacent amino acids will present on alternate sides of the pleated β-sheets (Figure 1).

Aqueous samples (0.5 wt %) were prepared by direct dispersion of the molecules in milli-Q water, using an aqueous NaOH solution (1 mM) to promote solvation and to help adjust solution pH close to neutral. In order to eliminate possible kinetic effects on the self-assembled nanostructures, all the solution samples were aged for at least 2 weeks at room temperature (unless specified otherwise). Cryogenic transmission electron microscopy (cryo-TEM) was used to characterize the self-assembled nanostructures. As shown in Figure 2, **VEVE** assembles into a nanobelt morphology with an average width of ∼140 nm, and **EVEV** forms a twisted ribbon morphology with an average width of ∼60 nm (Figure 2C), nearly half the width of the **VEVE** nanobelts. Interestingly, dramatic morphological changes were observed when the positions of the two middle amino acids are switched from VEVE to VVEE or from EVEV to EEVV. Figure 2B and 2D reveal nanofibers with a diameter of ∼9 nm and ∼18 nm, respectively. It is noteworthy that cylindrical nanofibers of **VVEE** (Figure 2B) appear rigid and tend to align into ordered domains while nanofibers of **EEVV** (Figure 2D) seem more flexible and entangle into a random network. Given that our CD measurements revealed a β-sheet conformation for all the peptide amphiphiles, it is evident that the 1D nature of all the

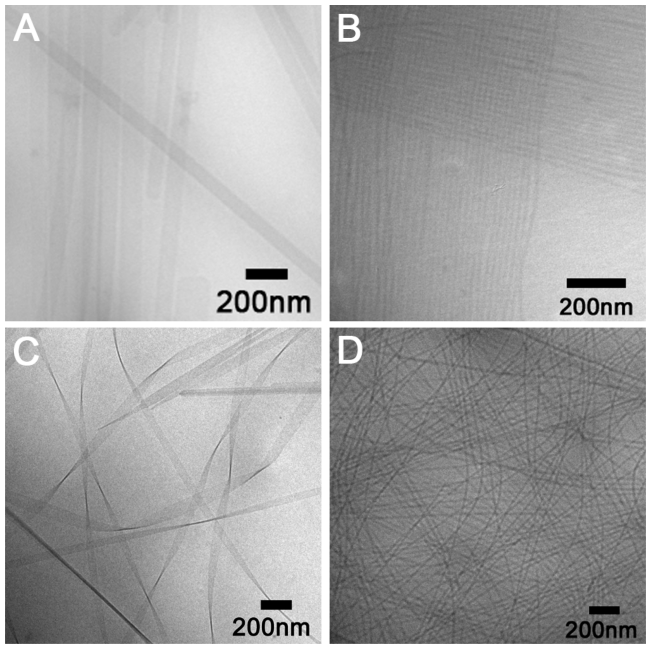

Figure 2. Cryo-TEM images of a variety of 1D nanostructures formed by the designed peptides in water after 2 weeks of incubation at room temperature. (A) Nanobelts of **VEVE**; (B) rigid cylindrical nanofibers of **VVEE**; (C) twisted nanoribbons of **EVEV**; (D) flexible and entangled nanofibers of **EEVV**.

morphologies observed here is linked to the intermolecular hydrogen bonding among peptide segments that drives the self-assembly of molecules preferentially in one dimension. At the same time, the structural/morphological difference must be rooted in the intermolecular interactions between side chains that apparently depend on the amino acid sequence.

We propose that the observed supramolecular architecture can be reasonably interpreted from two principles of molecular design. First, molecules with an alternating sequence of hydrophobic and hydrophilic amino acids, as in **VEVE** and **EVEV**, always form flat nanostructures lacking curvature. This flatness could be attributed to the dimerization of two molecules caused by association of the hydrophobic valine surface.[25] These dimerized molecules with two alkyl tails tend to further assemble into a flat morphology that eliminates the interfacial curvature between the peptide segments and the alkyl tails, in a way similar to the formation of vesicular assemblies by lipid molecules. Disruption of this structural motif leads to the formation of cylindrical nanofibers resulting from the combination of alkyl tail-induced hydrophobic collapse and intermolecular hydrogen bonding among peptide segments. This observation is consistent with our previous reports on other PA systems.[20,42] Second, the first amino acid connected to the alkyl tail plays a critical role in determining the final self-assembled nanostructures. When the glutamic acid was placed next to the alkyl chain, it is very likely that a steric effect and electrostatic repulsions among side chains of glutamic acid are enhanced at the peptide−alkane interface. These strengthened repulsive interactions among peptide segments have a greater effect on the internal packing of molecules within the 1D assemblies. The structural transitions from flat nanobelts to twisted ribbons and from rigid cylinders to flexible cylinders reflect these effects. Mezzenga and co-workers have reported that screening the electrostatic repulsions by increasing solution ionic strengths could lead to an increase in

dx.doi.org/10.1021/ja507051w | J. Am. Chem. Soc. 2014, 136, 12461−12468

the periodic pitch of protein fibrils, and they suggested that the twisted fibril morphology is a result of balancing electrostatic repulsions with the elastic energy penalty associated with fibril twists.[49,50] In the case of the **EVEV** sequence reported here, the increased repulsions likely limit the lateral growth of the assembled structures, leading to formation of relatively narrower, and thus, twisted 1D architectures.

Wide-Angle X-ray Diffraction of VEVE and EVEV Assemblies. To understand the difference of how peptide molecules are packed within the **VEVE** nanobelts and the **EVEV** twisted ribbons, we performed X-ray diffraction experiments on their aqueous solutions. In order to align these fibrillar assemblies to a preferred direction for oriented fiber diffractions, a narrow needle mounted on a plastic syringe was used to apply a shear force when loading the liquid samples into the quartz capillaries. Samples prepared this way, although not perfectly aligned, are oriented enough to offer a diffraction difference in intensity along and perpendicular to the direction of alignment. Figure 3A and 3B demonstrate the resulting 2D

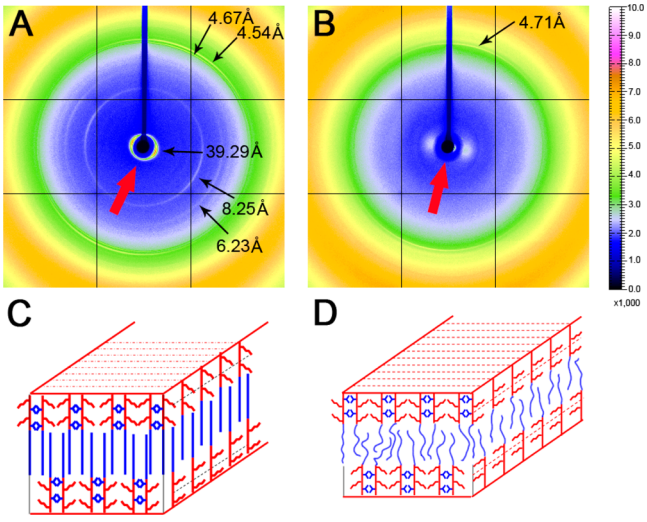

Figure 3. 2-D X-ray diffraction patterns from **VEVE** (A) and **EVEV** (B) nanostructures in aqueous solutions, and the proposed molecular packing models for **VEVE** nanobelts (C) and **EVEV** twisted ribbons (D).

diffraction patterns collected from 2.5 wt % aqueous solutions of **VEVE** nanobelts and **EVEV** twisted ribbons, respectively, with the red arrows pointing to the alignment direction. Clearly, the multiple diffraction peaks observed in Figure 3A suggest that nanobelts are highly crystalline. The observation of the nanobelt diffraction pattern is consistent with our proposed model illustrated in Figure 3C. First, the outermost doublet peaks at 4.67 and 4.54 Å are attributed to the higher order reflections of the periodic spacings associated with the intermolecular hydrogen bonding between peptide segments. Although this reflection often varies slightly around the spacing of 4.7 Å depending on side chain interactions, it has been frequently reported in many amyloid and peptide fibrillar assemblies and is generally considered to be typical of the β-sheet secondary structure.[51−54] Second, the strong, innermost reflection corresponds to a d spacing of 39.29 Å and its intensity is enhanced in the direction perpendicular to the corresponding β-sheet diffraction arcs. We attribute this reflection to the regular stacking along the Z-direction of the nanobelt because the value of ∼4 nm is reasonably close to the projected height of the interdigitated nanobelt and is in agreement with our previous neutron scattering results.[25] Third, two additional reflections were observed in parallel with the arcs of the 39.29 Å reflection. These two reflections correspond to d spacings of 8.25 and 6.23 Å, respectively, and are attributed to the third (300) and fourth order (400) reflections of the ∼25 Å spacing (100).[12,52,55] This ∼25 Å spacing correlates well to the expected width of the **VEVE** dimer with fully extended side chains[25] and has been regarded by Pochan and co-workers as the periodic spacing of the width of two stacked β-sheets as a result of the hydrophobic collapse of valine surfaces in their peptide assembly system.[12] Therefore, it is very likely that alkyl tails within the nanobelts are packed in a very ordered fashion, as illustrated in Figure 3C.

The crystalline structure observed within the nanobelts is in contrast to the molecular packing order within the twisted ribbons, as illustrated by our X-ray diffraction results. For the 2.5 wt % **EVEV** twisted ribbon aqueous solution, X-ray diffraction experiments only reveal one reflection peak at 4.71 Å corresponding to the expected β-sheet conformation of the peptide segment. This observation suggests that **EVEV** molecules are likely packed more loosely within the twisted ribbons (Figure 3D). These X-ray diffraction studies clearly demonstrate the significance of placing the bulkier, chargeable glutamic acid residue at the peptide−alkane interface and how such a change can influence the way in which the molecules are ordered within their respective assemblies.

Structural Evolution of EVEV 1D Nanostructures. Interestingly, after aging the **EVEV** aqueous solution for 2 months, we observed that some twisted ribbons (Figure 4A)

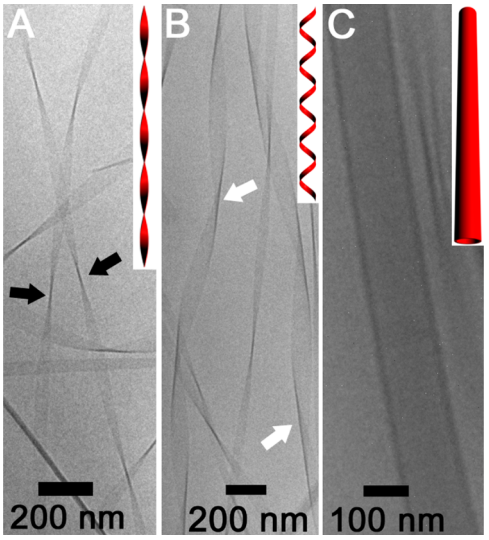

Figure 4. Kinetically controlled structural evolution from dominant twisted ribbons formed after 2 weeks of incubation (A) to helical ribbons (B) and nanotubes (C) after aging a 0.5% aqueous solution of **EVEV** for 2 months. Black and white arrows mark the darkest region of twisted ribbons and helical ribbons, respectively.

had transformed into helical ribbons (Figure 4B). On occasion, nanotubes could be also observed coexisting with the helical ribbons and twisted ribbons (Figure 4C). The existence of helical ribbons can be easily identified from the contrast variation in cryo-TEM micrographs. Folded edges of the helical ribbons appear to be the darkest areas of the structure (marked with white arrows in Figure 4B), while in twisted ribbons the

dx.doi.org/10.1021/ja507051w | J. Am. Chem. Soc. 2014, 136, 12461−12468

darkest regions are located in the center (marked with black arrows in Figure 4A). It is important to note here that **VEVE** nanobelts did not show any signs of transforming into either helical ribbons or nanotubes, even after the solution was aged for more than 6 months.

The structural transition from twisted ribbons to helical ribbons is indicative of a change in the packing order within the nanostructures. For the self-assembly of chiral molecules such as peptides, high-curvature nanostructures, such as cylindrical tubes, twisted ribbons, or helical ribbons, have been observed much more frequently compared to the low-curvature structures, such as flat membranes or nanobelts.[28,47,44,56,57] At the nanoscale, a helical ribbon differs from a twisted ribbon in the fact that helical ribbons have a cylindrical curvature while twisted ribbons have a Gaussian or saddle-like curvature.[50,58] Whether helical ribbons or twisted ribbons are formed as a result of chiral assembly is dependent upon the membrane's (or the belt's) bending modulus, a property that is a function of the internal molecular packing (crystalline or fluid-like) and the thickness of the ribbon.[59] Oda et al. have shown that membranes with more ordered internal structures tend to form helical ribbons rather than twisted ribbons.[60] There is also speculation that membranes of multiple bilayers (a greater thickness) prefer helical ribbons over twisted ribbons.[50,59] In the case reported here, we consider the observed structural transition to be a result of changes in the internal packing order among alkyl tails because the twisted ribbons and helical ribbons did not show any noticeable differences in thickness and also because X-ray diffraction experiments (Figure 3B) revealed a much less ordered internal structure within the **EVEV** twisted ribbons.

We believe that placing the glutamic acid with its chargeable, bulkier side chain at the interface changes not only the balance of forces in the interfacial area but also the packing kinetics of the self-assembled nanostructures. Presumably, the enhanced steric and electrostatic repulsions among glutamic acid side chains will not allow the alkyl tails of **EVEV** to pack as tightly as the alkyl tails of **VEVE** do within the nanobelts, where a valine actually serves as a spacer between the tail and the glutamic acid residue. Therefore, in response to the increased distance between **EVEV** molecules, the alkyl tails must be less stretched in order to occupy the physical volume within the nanostructure core. The X-ray diffraction results in Figure 3A and 3B prove that alkyl tails of **EVEV** are indeed packed more loosely within the twisted ribbons. Given time, the alkyl chains may slowly rearrange into a more ordered fashion, likely accompanied by some corresponding chain conformation adjustment of the **EVEV** peptide segment, and thus leading to the formation of helical ribbons. Unfortunately, our X-ray diffraction experiments did not reveal any noticeable difference between the **EVEV** samples aged for 2 weeks and aged for 2 months, possibly due to the small percentage of helical ribbons formed within the solution that did not give enough crystalline scattering. Helical ribbons have been reported to be potential precursors for the formation of nanotubes,[59] and we could on occasion observe the nanotube morphology coexisting with helical and twisted ribbons (Figure 4C). This observation of rearranging molecular segments within its own self-assembled structures resembles the process of protein folding, in which multiple folding steps are often involved before reaching the stable state. The folding kinetics are of critical importance in defining a protein's final tertiary structure and would appear to play an important role in the structures adopted by peptide amphiphiles.

Nanofibers of VVEE and EEVV. Closer examination of the nanofiber structures of **VVEE** and **EEVV** reveals that they are two distinct types of nanofibers. The 9 nm diameter of nanofibers formed by **VVEE** is reasonably close to the expected value of a core−shell cylindrical structure. This morphology is typical of PA nanofibers as reported previously in other systems.[20] Obviously, the 18 nm diameter of the nanofibers formed by the **EEVV** is more than twice that of the fully extended molecular length and therefore cannot be explained by the simple core−shell model. Rather, it suggests a more complex 1D nanostructure. Both negatively stained TEM (Figure 5A) and cryo-TEM micrographs (Figure 5B)

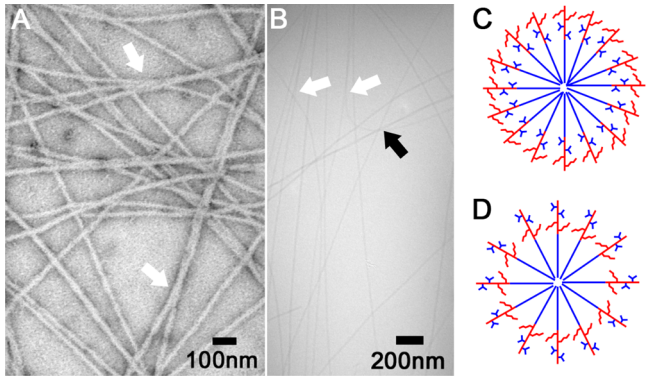

Figure 5. (A) Cast-film TEM image of **EEVV** nanofibers (the sample was negatively stained with an aqueous uranyl acetate solution), and (B) cryo-TEM image of **EEVV** nanofibers. White arrows mark the locations where bundled nanofibers split into two separate narrower nanofibers (Figure S3 offers a high resolution image of Figure 5B). The black arrow in (B) marks a nanofiber of a larger diameter. (C) and (D) reveal the proposed molecular packing models in **VVEE** and **EEVV**, respectively.

demonstrate that the **EEVV** nanofibers are composed of smaller 1D nanostructures. It can be clearly seen in Figure 5A that two narrower nanofibers intertwine together into a larger one (marked with white arrows). Moreover, the variation in diameter further supports the observation that **EEVV** nanofibers consist of different numbers of smaller aggregates.

Nanofibers of **VVEE** and **EEVV** were further studied by small-angle X-ray scattering experiments. As shown in Figure 6, the nanofiber morphology was inferred by the −1 slope in the low q region and the form factor peaks around 0.1 $Å^{-1}$. The scattering profile of **EEVV** nanofibers can be fitted into the form factor model calculated for flexible cylinders with a polydisperse radius, giving an average radius of 7.9 nm. However, the scattering curve of **VVEE** cannot be fit to any form factor models of cylindrical objects possibly due to the influence of the structural factor among these bundled fibers (Figure 2B). As is seen in Figure 6, the slope of the scattering spectrum of **VVEE** nanofibers is slightly higher than −1, a deviation that could arise from the interactions among nanofibers that enhance the scattering intensity in the low q region. Therefore, the diameter of the **VVEE** nanofibers was estimated using the first minima of the scattering spectra without detailed modeling.[61] For the scattering of cylindrical objects, the first-order Bessel function $J_1(qR_c) = 0$, where the q value is the position of the form factor minima and R_c is the cross section radius. This crude estimate gives rise to 3.9 and

dx.doi.org/10.1021/ja507051w | J. Am. Chem. Soc. 2014, 136, 12461−12468

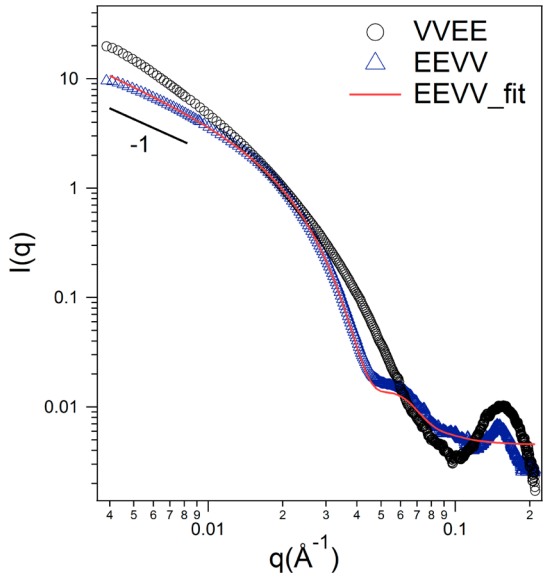

Figure 6. Small angle X-ray scattering (SAXS) spectra of 0.5 wt % aqueous solutions of **EEVV** and **VVEE**. The scattering profile of **EEVV** nanofibers can be fit into a form factor model calculated for flexible cylinders with a polydisperse radius.

7.7 nm for the **VVEE** and **EEVV** fibrillar assemblies, respectively. These values are in good agreement with our cryo-TEM data.

We envision that the intertwined nanofibers in **EEVV** originate from the structure of the protofilaments (early stage 1D assemblies) that expose the hydrophobic valines to water. Presumably, **EEVV** also prefers to form a core–shell cylindrical morphology (Figure 5D) as a result of its amphiphilic nature. The tendency to minimize the exposure of hydrophobic valine surfaces to water leads to the association, or fusion of these protofilaments. As a consequence, formation of these fused and interweaved nanofibers significantly increases the solution viscosity. In fact, a self-supporting hydrogel was observed at 1 wt % **EEVV** aqueous solution in the absence of any salts. Rheology measurements show that the storage modulus could reach up to 200 Pa (Figure S4), in contrast to the nanofibers of **VVEE** that could form robust gels only when $CaCl_2$ is added. The entanglement mechanism in the **EEVV** nanofiber network perhaps provides an interesting means for constructing robust hydrogels, and the resultant materials may offer a useful matrix for cell culture since their gelation process does not require the addition of multivalent counterions.[62]

RGD Incorporation. In order to explore the potential biological applications of these 1D nanostructures, we

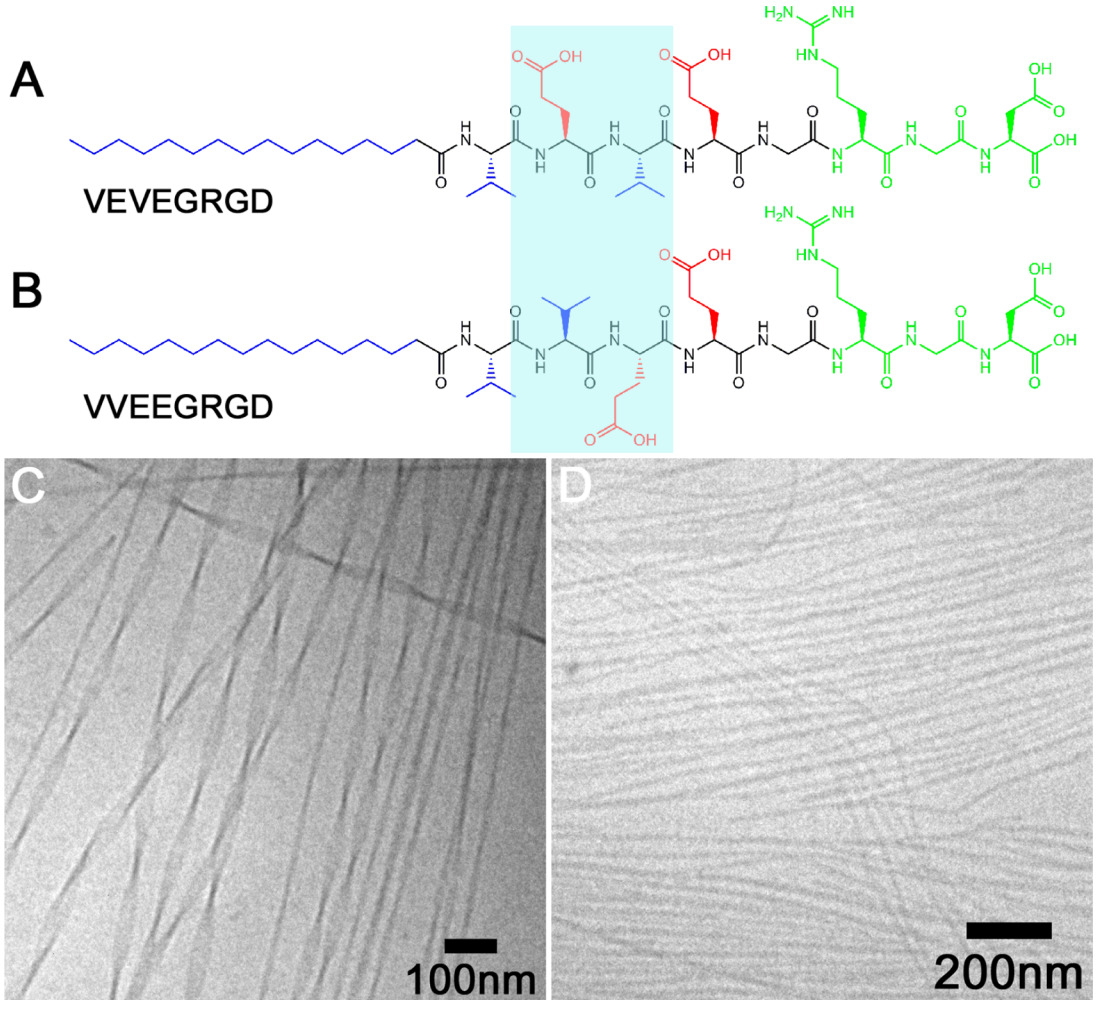

Figure 7. Molecular structure of **VEVEGRGD** (A) and **VVEEGRGD** (B); (C) Cryo-TEM image of twisted ribbons of **VEVEGRGD** at 0.5 wt % aqueous solution and (D) cryo-TEM image of nanofibers of **VVEEGRGD** at 0.5 wt % aqueous solution. In both cases, the TEM images were taken after 2 weeks of incubation at room temperature.

dx.doi.org/10.1021/ja507051w | J. Am. Chem. Soc. 2014, 136, 12461–12468

incorporated the Arg-Gly-Asp (RGD) peptide sequence into the molecular design to enhance their interactions with cells.[25,63] Importantly, we found that these nanostructures are able to maintain their shapes even with the extended RGD sequence. As is shown in Figure 7, the molecule with **VEVEGRGD** sequence forms twisted ribbons (Figure 7C) that resemble the nanobelt morphology of **VEVE**, while **VVEEGRGD** forms cylindrical nanofibers (Figure 7D) similar to the **VVEE** nanofibers. It is very interesting that the dramatic change in self-assembled structures is solely dictated by switching the positions of two adjacent amino acids in the middle domain of the eight-residue peptide, allowing the architecture of the nanostructures to be varied while still presenting a biological signaling sequence in the terminal domain.

CONCLUSIONS

We have reported on four different types of self-assembled 1D nanostructures resulting from the self-assembly of isomeric tetrapeptide amphiphiles with identical composition but a different sequence of amino acids. Our results clearly demonstrate the significance of side chain interactions in determining the self-assembled supramolecular architectures of small peptides. The observations should encourage more systematic studies on the use of peptide-based constitutional isomers to create supramolecular functional assemblies which may have unique functions given that they are formed by molecules of the same composition. For instance, the bioactive RGD peptide sequence is likely presented with a different packing density on the surfaces of **VEVEGRGD** and **VVEEGRGD** assemblies, and this may impact directly cell adhesion behavior. The nanofibers formed by **VVEE** and **EEVV** entangle into hydrogels with different mechanical properties, and this could in turn be used to control stem cell differentiation. The ultimate goal is to precisely design the desired biological functions of peptide supramolecular materials through composition and sequence control of their amino acid structural units.

ASSOCIATED CONTENT

Supporting Information

Details of molecular characterization, circular dichroism studies, additional cryo-TEM images, and rheology results and experimental procedures can be found in online supporting material. This material is available free of charge via the Internet at http://pubs.acs.org.

AUTHOR INFORMATION

Corresponding Author

s-stupp@northwestern.edu

Present Address

[#]Department of Chemical and Biomolecular Engineering, Johns Hopkins University, Baltimore, MD 21218, United States

Notes

The authors declare no competing financial interest.

ACKNOWLEDGMENTS

This work was supported by the National Science Foundation Grant DMR-1006713. The authors are grateful to Biological Imaging Facility (BIF) and Keck Biophysics Facility at Northwestern University. Peptide synthesis and ESI-MS were performed in the Chemistry Core Facility of the Institute for BioNanotechnology in Medicine at Northwestern University. The U.S. Army Research Office, the U.S. Army Medical Research and Materiel Command, and Northwestern University provided funding to develop this facility. The wide-angle X-ray diffraction (WAXS) experiments were performed at the BioCARS Sector 14 of the Advanced Photon Source (APS), Argonne National Lab. Use of the BioCARS Sector 14 was supported by the National Institutes of Health, National Center for Research Resources, under Grant Number RR007707. Small-angle X-ray scattering experiments were performed at the DuPont-Northwestern-Dow Collaborative Access Team (DND-CAT) located at Sector 5 of the Advanced Photon Source. DND-CAT is supported by E.I. DuPont de Nemours & Co., The Dow Chemical Company, and the State of Illinois. Use of the Advanced Photon Source was supported by the U.S. Department of Energy, Basic Energy Sciences, Office of Science, under Contract No. DE-AC02-06CH11357.

REFERENCES

(1) Beniash, E.; Hartgerink, J. D.; Storrie, H.; Stendahl, J. C.; Stupp, S. I. *Acta Biomaterialia* **2005**, *1*, 387−397.
(2) Cui, H. G.; Webber, M. J.; Stupp, S. I. *Biopolymers* **2010**, *94*, 1−18.
(3) Hamley, I. W. *Biomacromolecules* **2014**, *15*, 1543−1559.
(4) Lin, Y. A.; Ou, Y. C.; Cheetham, A. G.; Cui, H. G. *Biomacromolecules* **2014**, *15*, 1419−1427.
(5) Silva, G. A.; Czeisler, C.; Niece, K. L.; Beniash, E.; Harrington, D. A.; Kessler, J. A.; Stupp, S. I. *Science* **2004**, *303*, 1352−1355.
(6) Stupp, S. I.; Zha, R. H.; Palmer, L. C.; Cui, H. G.; Bitton, R. *Faraday Discuss.* **2013**, *166*, 9−30.
(7) Zhou, J.; Du, X. W.; Gao, Y.; Shi, J. F.; Xu, B. *J. Am. Chem. Soc.* **2014**, *136*, 2970−2973.
(8) Aggeli, A.; Nyrkova, I. A.; Bell, M.; Harding, R.; Carrick, L.; McLeish, T. C. B.; Semenov, A. N.; Boden, N. *Proc. Natl. Acad. Sci. U.S.A.* **2001**, *98*, 11857−11862.
(9) Borner, H. G.; Smarsly, B. M.; Hentschel, J.; Rank, A.; Schubert, R.; Geng, Y.; Discher, D. E.; Hellweg, T.; Brandt, A. *Macromolecules* **2008**, *41*, 1430−1437.
(10) Debnath, S.; Roy, S.; Ulijn, R. V. *J. Am. Chem. Soc.* **2013**, *135*, 16789−16792.
(11) Kuang, Y.; Gao, Y.; Shi, J. F.; Li, J.; Xu, B. *Chem. Commun.* **2014**, *50*, 2772−2774.
(12) Lamm, M. S.; Rajagopal, K.; Schneider, J. P.; Pochan, D. J. *J. Am. Chem. Soc.* **2005**, *127*, 16692−16700.
(13) Lashuel, H. A.; LaBrenz, S. R.; Woo, L.; Serpell, L. C.; Kelly, J. W. *J. Am. Chem. Soc.* **2000**, *122*, 5262−5277.
(14) Meijer, J. T.; Roeters, M.; Viola, V.; Lowik, D.; Vriend, G.; van Hest, J. C. M. *Langmuir* **2007**, *23*, 2058−2063.
(15) Wu, D. D.; Zhou, J.; Shi, J. F.; Du, X. W.; Xu, B. *Chem. Commun.* **2014**, *50*, 1992−1994.
(16) Yu, T. B.; Bai, J. Z.; Guan, Z. B. *Angew. Chem., Int. Ed.* **2009**, *48*, 1097−1101.
(17) Abul-Haija, Y. M.; Roy, S.; Frederix, P.; Javid, N.; Jayawarna, V.; Ulijn, R. V. *Small* **2014**, *10*, 973−979.
(18) Cui, H. G.; Pashuck, E. T.; Velichko, Y. S.; Weigand, S. J.; Cheetham, A. G.; Newcomb, C. J.; Stupp, S. I. *Science* **2010**, *327*, 555−559.
(19) Guler, M. O.; Soukasene, S.; Hulvat, J. F.; Stupp, S. I. *Nano Lett.* **2005**, *5*, 249−252.
(20) Hartgerink, J. D.; Beniash, E.; Stupp, S. I. *Science* **2001**, *294*, 1684−1688.
(21) Lin, R.; Cheetham, A. G.; Zhang, P. C.; Lin, Y. A.; Cui, H. G. *Chem. Commun.* **2013**, *49*, 4968−4970.
(22) Pomerantz, W. C.; Yuwono, V. M.; Pizzey, C. L.; Hartgerink, J. D.; Abbott, N. L.; Gellman, S. H. *Angew. Chem., Int. Ed.* **2008**, *47*, 1241−1244.

(23) Zhang, P. C.; Cheetham, A. G.; Lin, Y. A.; Cui, H. *ACS Nano* **2013**, *7*, 5965−5977.
(24) Li, L. S.; Jiang, H. Z.; Messmore, B. W.; Bull, S. R.; Stupp, S. I. *Angew. Chem., Int. Ed.* **2007**, *46*, 5873−5876.
(25) Cui, H.; Muraoka, T.; Cheetham, A. G.; Stupp, S. I. *Nano Lett.* **2009**, *9*, 945−951.
(26) Fishwick, C. W. G.; Beevers, A. J.; Carrick, L. M.; Whitehouse, C. D.; Aggeli, A.; Boden, N. *Nano Lett.* **2003**, *3*, 1475−1479.
(27) Lin, Y. A.; Ou, Y. C.; Cheetham, A. G.; Cui, H. G. *ACS Macro Lett.* **2013**, *2*, 1088−1094.
(28) Castelletto, V.; Hamley, I. W.; Hule, R. A.; Pochan, D. *Angew. Chem., Int. Ed.* **2009**, *48*, 2317−2320.
(29) Marini, D. M.; Hwang, W.; Lauffenburger, D. A.; Zhang, S. G.; Kamm, R. D. *Nano Lett.* **2002**, *2*, 295−299.
(30) Moyer, T. J.; Cui, H. G.; Stupp, S. I. *J. Phys. Chem. B* **2013**, *117*, 4604−4610.
(31) Smith, A. M.; Williams, R. J.; Tang, C.; Coppo, P.; Collins, R. F.; Turner, M. L.; Saiani, A.; Ulijn, R. V. *Adv. Mater.* **2008**, *20*, 37−41.
(32) Tang, C.; Ulijn, R. V.; Saiani, A. *Langmuir* **2011**, *27*, 14438−14449.
(33) Bucak, S.; Cenker, C.; Nasir, I.; Olsson, U.; Zackrisson, M. *Langmuir* **2009**, *25*, 4262−4265.
(34) Cheetham, A. G.; Zhang, P. C.; Lin, Y. A.; Lock, L. L.; Cui, H. G. *J. Am. Chem. Soc.* **2013**, *135*, 2907−2910.
(35) Hamley, I. W. *Angew. Chem., Int. Ed.* **2014**, *53*, 6866−6881.
(36) Hartgerink, J. D.; Granja, J. R.; Milligan, R. A.; Ghadiri, M. R. *J. Am. Chem. Soc.* **1996**, *118*, 43−50.
(37) Liu, P.; Ni, R.; Mehta, A. K.; Childers, W. S.; Lakdawala, A.; Pingali, S. V.; Thiyagarajan, P.; Lynn, D. G. *J. Am. Chem. Soc.* **2008**, *130*, 16867−16869.
(38) Reches, M.; Gazit, E. *Nat. Nanotechnol.* **2006**, *1*, 195−200.
(39) Boekhoven, J.; Stupp, S. I. *Adv. Mater.* **2014**, *26*, 1642−1659.
(40) Korevaar, P. A.; Newcomb, C. J.; Meijer, E. W.; Stupp, S. I. *J. Am. Chem. Soc.* **2014**, *136*, 8540−8543.
(41) Newcomb, C. J.; Sur, S.; Ortony, J. H.; Lee, O. S.; Matson, J. B.; Boekhoven, J.; Yu, J. M.; Schatz, G. C.; Stupp, S. I. *Nat. Commun.* **2014**, *5*, doi: 10.1038/ncomms4321.
(42) Velichko, Y. S.; Stupp, S. I.; de la Cruz, M. O. *J. Phys. Chem. B* **2008**, *112*, 2326−2334.
(43) Pashuck, E. T.; Cui, H. G.; Stupp, S. I. *J. Am. Chem. Soc.* **2010**, *132*, 6041−6046.
(44) Pashuck, E. T.; Stupp, S. I. *J. Am. Chem. Soc.* **2010**, *132*, 8819−8821.
(45) Marullo, R.; Kastantin, M.; Drews, L. B.; Tirrell, M. *Biopolymers* **2013**, *99*, 573−581.
(46) Lowik, D.; Shklyarevskiy, I. O.; Ruizendaal, L.; Christianen, P. C. M.; Maan, J. C.; van Hest, J. C. M. *Adv. Mater.* **2007**, *19*, 1191−1195.
(47) Nieuwland, M.; Ruizendaal, L.; Brinkmann, A.; Kroon-Batenburg, L.; van Hest, J. C. M.; Lowik, D. *Faraday Discuss.* **2013**, *166*, 361−379.
(48) Hamley, I. W.; Dehsorkhi, A.; Castelletto, V.; Furzeland, S.; Atkins, D.; Seitsonen, J.; Ruokolainen, J. *Soft Matter* **2013**, *9*, 9290−9293.
(49) Adamcik, J.; Mezzenga, R. *Soft Matter* **2011**, *7*, 5437−5443.
(50) Adamcik, J.; Mezzenga, R. *Macromolecules* **2012**, *45*, 1137−1150.
(51) Kirschner, D. A.; Abraham, C.; Selkoe, D. J. *Proc. Natl. Acad. Sci. U.S.A.* **1986**, *83*, 503−507.
(52) Makin, O. S.; Serpell, L. C. *FEBS J.* **2005**, *272*, 5950−5961.
(53) Nguyen, J. T.; Inouye, H.; Baldwin, M. A.; Fletterick, R. J.; Cohen, F. E.; Prusiner, S. B.; Kirschner, D. A. *J. Mol. Biol.* **1995**, *252*, 412−422.
(54) Sunde, M.; Blake, C. *Adv. Protein Chem.* **1997**, *50*, 123−159.
(55) Sunde, M.; Serpell, L. C.; Bartlam, M.; Fraser, P. E.; Pepys, M. B.; Blake, C. C. F. *J. Mol. Biol.* **1997**, *273*, 729−739.
(56) Ziserman, L.; Lee, H. Y.; Raghavan, S. R.; Mor, A.; Danino, D. *J. Am. Chem. Soc.* **2011**, *133*, 2511−2517.
(57) Ziserman, L.; Mor, A.; Harries, D.; Danino, D. *Phys. Rev. Lett.* **2011**, *106*, 4.
(58) Shimizu, T.; Masuda, M.; Minamikawa, H. *Chem. Rev.* **2005**, *105*, 1401−1443.
(59) Selinger, J. V.; Spector, M. S.; Schnur, J. M. *J. Phys. Chem. B* **2001**, *105*, 7157−7169.
(60) Oda, R.; Huc, I.; Schmutz, M.; Candau, S. J.; MacKintosh, F. C. *Nature* **1999**, *399*, 566−569.
(61) Bang, J.; Jain, S. M.; Li, Z. B.; Lodge, T. P.; Pedersen, J. S.; Kesselman, E.; Talmon, Y. *Macromolecules* **2006**, *39*, 1199−1208.
(62) Stendahl, J. C.; Rao, M. S.; Guler, M. O.; Stupp, S. I. *Adv. Funct. Mater.* **2006**, *16*, 499−508.
(63) Webber, M. J.; Tongers, J.; Renault, M. A.; Roncalli, J. G.; Losordo, D. W.; Stupp, S. I. *Acta Biomaterialia* **2010**, *6*, 3−11.